Copy
RM SL55B07

RESEARCH MEMORANDUM

for the

U. S. Air Force

TRANSONIC FREE-FLIGHT INVESTIGATION OF THE LONGITUDINAL AERODYNAMIC CHARACTERISTICS OF A 1/10-SCALE STEEL-WING MODEL OF THE NORTHROP MX-775A MISSILE WITH LEADING-EDGE EXTENSIONS, INBOARD TRAILING-EDGE FLAPS, AND A SPEED BRAKE ON THE VERTICAL TAIL

By Richard G. Arbic

Langley Aeronautical Laboratory
Langley Field, Va.

NATIONAL ADVISORY COMMITTEE FOR AERONAUTICS

WASHINGTON

NACA RM SL55B07

NATIONAL ADVISORY COMMITTEE FOR AERONAUTICS

RESEARCH MEMORANDUM

for the

U. S. Air Force

TRANSONIC FREE-FLIGHT INVESTIGATION OF THE LONGITUDINAL AERODYNAMIC CHARACTERISTICS OF A 1/10-SCALE STEEL-WING MODEL OF THE NORTHROP MX-775A MISSILE WITH LEADING-EDGE EXTENSIONS, INBOARD TRAILING-EDGE FLAPS, AND A SPEED BRAKE ON THE VERTICAL TAIL

By Richard G. Arbic

SUMMARY

Results are presented of a free-flight investigation between Mach numbers of 0.7 to 1.3 and Reynolds numbers of 3.1×10^6 to 7.0×10^6 to determine the longitudinal aerodynamic characteristics of the Northrop MX-775A missile. This missile has a wing, body, and vertical tail, but has no horizontal tail. The basic wing plan form has an aspect ratio of 5.5, 45° of sweepback of the 0.406 streamwise chord line, and a taper ratio of 0.4. A 1/10-scale steel-wing model of the missile was flown with modifications to the basic wing plan form consisting of leading-edge chord-extensions deflected 7° downward together with the forward 15 percent of the wing chord, and inboard trailing-edge flaps deflected 5° downward. In addition, the model had a static-pressure tube mounted at the tip of the vertical tail for position-error measurements and had a speed brake also mounted on the vertical tail to trim the model to positive lift coefficients and to permit determination of the trim and drag effectiveness of the brake. The data are uncorrected for the effects of wing elasticity, but experimental wing influence coefficients are presented.

The significant results of this investigation were as follows. The speed brake accounted for 55 percent of the subsonic minimum drag of the configuration and for 32 percent at a Mach number of 1.2. In addition, the speed-brake resulted in more positive trim, changing the trim angle

of attack by 1° to 1.5° and the trim lift coefficient by approximately 0.1 although the trim angle of attack remained negative. The maximum value of lift coefficient for zero angle of attack was 0.2 near a Mach number of 0.96. Nonlinearities in the lift-curves for the transonic Mach numbers resulted in decreasing values of the lift-curve slope with increasing lift coefficient. Movement of the aerodynamic center was from 27 percent of the mean aerodynamic chord at subsonic Mach numbers to 42 percent at a Mach number of 1.2. The configuration exhibited stable total damping characteristics although the sum of the pitch-damping derivatives was unstable in the transonic speed range. The location of the static-pressure tube resulted in severe errors in static pressure for Mach numbers between 0.9 and 1.25 and in moderate to small errors for the lower Mach numbers.

INTRODUCTION

At the request of the United States Air Force, the Langley Pilotless Aircraft Research Division is investigating the transonic low-lift aerodynamic characteristics of the Northrop long-range surface-to-surface missile designated MX-775A. This missile is designed to cruise at high subsonic Mach numbers and to attain supersonic speeds during the terminal approach to the target. The missile has a wing, body, and vertical tail, but has no horizontal tail. Longitudinal controls are on the wing which is mounted high on the body.

This paper presents the results of one of a series of rocket-model tests of the MX-775A configuration. The present test model had a steel-wing with wing modifications consisting of a drooped leading edge, drooped leading-edge extensions, and deflected inboard trailing-edge flaps. In addition, the model had a static-pressure tube and a speed brake, both mounted on the vertical tail. The purpose of the static-pressure tube was to obtain position-error measurements since the missile autopilot uses airspeed and altitude as primary longitudinal control quantities. The speed brake was used to trim the model to more positive lift coefficients and to obtain trim and drag data. Lift, drag, and pitching-moment data are presented together with the trim characteristics of the missile, and static-pressure measurements from the tube are compared with radiosonde static pressure. Rocket model data from an identical model without the speed brake and with an aluminum-alloy wing (ref. 1) are presented for comparison of trim and drag. Some data made available to the National Advisory Committee for Aeronautics from the Wright Air Development Center (WADC) 10-foot wind tunnel are also presented. Additional rocket-model tests of the MX-775A configuration are presented in references 2 and 3. Wright Air Development Center and Ames wind-tunnel tests are presented in references 4 and 5, respectively.

[redacted]

The present flight test was conducted at the Langley Pilotless Aircraft Research Station at Wallops Island, Va.

SYMBOLS

The coefficients are based on the total area and mean aerodynamic chord of the basic wing plan form (no leading- or trailing-edge extensions).

a_l	longitudinal acceleration, ft/sec^2
a_n	normal acceleration, ft/sec^2
A	aspect ratio
b	wing span, ft
c	local wing chord, ft
c.g.	center-of-gravity position, positive to rear of leading edge of $\bar{c}$, percent $\bar{c}$
$\bar{c}$	mean aerodynamic chord of basic wing, 0.82 ft
C_C	chord-force coefficient, $\frac{-Wa_l}{gqS}$
C_D	drag coefficient, $C_C \cos \alpha + C_N \sin \alpha$
C_L	lift coefficient, $C_N \cos \alpha - C_C \sin \alpha$
C_{L_α}	lift-curve slope per degree, $\frac{\partial C_L}{\partial \alpha}$
C_m	pitching-moment coefficient, $\frac{I_y \ddot{\theta}}{qS\bar{c}}$
C_{m_α}	pitching-moment curve slope per degree, $\frac{\partial C_m}{\partial \alpha}$
C_N	normal-force coefficient, $\frac{Wa_n}{gqS}$
g	acceleration due to gravity, 32.2 ft/sec^2

[redacted]

I_y moment of inertia in pitch about the model center of gravity, slug-ft^2

L applied load, lb

M Mach number

P period, sec

q dynamic pressure

S total wing area of basic wing including portion within fuselage, 3.27 sq ft

$T_{1/2}$ time for oscillation to damp to one-half amplitude, sec

V flight-path velocity, ft/sec

W model weight, lb

y distance to any spanwise station from fuselage center line, ft

$\frac{y}{b/2}$ nondimensional wing spanwise parameter

α angle of attack, deg

$\dot{\alpha} = \frac{1}{57.3}\frac{d\alpha}{dt}$, radians/sec

θ angle of pitch, deg; also local wing twist angle, deg

$\dot{\theta} = \frac{1}{57.3}\frac{d\theta}{dt}$, radians/sec

$\ddot{\theta} = \frac{1}{57.3}\frac{d^2\theta}{dt^2}$, radians/sec^2

The pitch-damping derivatives are expressed as follows:

$$C_{m_q} = \frac{\partial C_m}{\partial \frac{\dot{\theta}\bar{c}}{2V}}$$

$$C_{m_{\dot{\alpha}}} = \frac{\partial C_m}{\partial \frac{\dot{\alpha}\bar{c}}{2V}}$$

MODEL AND INSTRUMENTATION

A three-view drawing of the model and details of the modifications to the basic wing plan form and to the vertical tail are shown in figure 1. The basic wing has an aspect ratio of 5.5, is swept back 45° at the 40.6-percent streamwise chord line, and has a taper ratio of 0.4. The airfoil of the basic wing is approximately 6 percent thick streamwise and is a Northrop modification of an NACA 65-009 section normal to the 40.6-percent streamwise chord line. Modifications to the basic wing plan form as used in the present test consisted of drooping the forward 15 percent (streamwise) of the wing leading-edge, addition of drooped leading-edge chord-extensions, and addition of inboard trailing-edge flaps. Both the chord-extensions and the wing leading edge were deflected 7° downward. The chord-extension overhang varied from 15 percent of the basic wing streamwise chord at 0.6 semispan to 0 percent at the wing tip. The trailing-edge flaps covered the inboard 36 percent of the wing trailing edge and were deflected 5° downward streamwise. Modifications to the vertical tail for the present test consisted of the addition of a speed brake (see fig. 1) and a static-pressure tube having four orifices (two in the vertical and two in the horizontal plane). The model wing was machined from steel and the vertical tail from magnesium. The fuselage was of sheet aluminum construction, had a fineness ratio of 13.94, and contained six pulse rockets for the purpose of disturbing the model in pitch. The model center of gravity was at 29.7 percent of the mean aerodynamic chord forward of the leading edge of the mean aerodynamic chord. Photographs of the model and of the model-booster combination are shown in figures 2 and 3. Table I presents the physical characteristics of the model, and table II lists the ordinates for the fuselage and the airfoil of the vertical tail, and for both the airfoil of the basic wing (modified NACA 65-009 section) and for the airfoil of the wing as modified by addition of leading-edge droop, leading-edge extensions, and trailing-edge flaps.

Model instrumentation consisted of a six-channel telemeter which transmitted continuous values of normal and longitudinal accelerations, angle of attack, pitching acceleration, static pressure (measured on a probe at the tip of the vertical tail), and total pressure.

TESTS AND CORRECTIONS

Structural influence coefficients were obtained for the steel wing by application of loads at five spanwise stations along the 40-percent-streamwise chord line. The influence coefficients thus obtained are presented in figure 4 to show the stiffness of the steel wing. Corrections for the effect of wing elasticity were not applied to the data

[redacted]

presented in this paper, but the influence coefficients in figure 4 will permit such a correction to be made.

The model was boosted to maximum velocity by an ABL Deacon rocket motor. Most of the data were obtained during coasting flight of the model following separation from the booster. The model was periodically disturbed in pitch by firing of the pulse rockets. Model velocity was obtained by use of both the CW Doppler radar unit and the telemetered total pressure. Doppler velocity was corrected for the effect of winds at altitude and was used for determination of Mach number and dynamic pressure. Trajectory data were calculated by making use of Doppler velocity and the flight-path angle at separation of the model from the booster. Free-stream temperature and static pressure, and the wind velocity at altitude were obtained from a radiosonde balloon.

The test conditions of Reynolds number and dynamic pressure are shown as a function of Mach number in figure 5. The Reynolds number range for the present test was 3.1×10^6 to 7.0×10^6, and the dynamic-pressure range varied from 500 to 2,300 pounds per square foot. The dynamic pressure is also shown for the WADC wind-tunnel test since lift and static stability from this test are compared with present test results in a later section.

ANALYSIS

The method of analysis of rocket-model data is described in general in reference 6, and the particular application to the present test is presented in references 1 and 2. Briefly, lift, drag, and longitudinal stability are obtained by analyzing short-period disturbances created by pulse rockets. Lift and drag are determined by resolving normal and longitudinal forces to the stability axes. Static stability is obtained from the period and damping of the oscillations and dynamic stability from the rate of decay of the oscillations.

ACCURACY

The estimated maximum probable errors for the test results are listed below based on accepted ranges of accuracy for the various instruments and experience from tests of identical models.

[redacted]

	M = 0.8	M = 1.2
Mach number	±0.010	±0.007
Angle of attack, deg	±0.28	±0.28
Lift coefficient	±0.02	±0.01
Drag coefficient	±0.003	±0.0015
Pitching-moment coefficient	±0.030	±0.015
Altitude, ft	±300	±100
Static pressure (from pressure tube), lb/sq in.	±0.2	±0.2

RESULTS AND DISCUSSION

Basic Data

A portion of the telemeter record is shown in figure 6 in order to discuss some conditions which affected the results obtained. These conditions are: (1) the breaks or nonlinearities in the pitching acceleration and (2) the superimposed oscillations on the trace of normal acceleration and to some extent on the traces of angle of attack and longitudinal acceleration. A detailed description of the possible source of these phenomena is presented in reference 1. Briefly, it is thought that the nonlinearities in the pitching acceleration are a result of flow separation at the leading edge of the airfoil and that the rapid change in pitching acceleration excites a wing-body bending mode. This mode had a frequency of approximately 57 cycles per second which corresponds to the frequency of the superimposed oscillations. Little was learned from the present test to confirm this supposition since the model carried essentially the same instrumentation as did the winged model of reference 1.

Figure 7 presents typical basic lift, drag, and pitching-moment data for the Mach number range from approximately 0.76 to 1.13. The effect of the nonlinearities noted in the pitching acceleration can be seen in the pitching-moment curves as hysteresis for the lift-coefficient range from approximately 0.1 to -0.2. This hysteresis is presumably due to separation and reattachment of the flow at the wing leading edge. It should be pointed out that due to the slow response characteristics of the angular accelerometer, the portions of the pitching-moment curves that show hysteresis should be examined in a qualitative manner only, since the instrument could not accurately follow abrupt changes in the pitching acceleration. Figure 7(c) is included to show that the low-amplitude data do not indicate separation, presumably because a sufficient negative lift coefficient was not reached. If this is the case, it is reasonable to assume that the full-scale missile will not experience the separation effects since these effects do not occur in the usable range of lift coefficients.

[redacted]

Although the lift curves in figure 7 are shown to be linear in the lift-coefficient range where separation is thought to have occurred, it was determined by filtering of the superimposed oscillations on the normal acceleration trace that a slight nonlinearity does exist in this region. However, the duration and relative amplitude of the nonlinearity were slight and could not be determined accurately from the filtered trace of normal acceleration due to the filter response characteristics, or by manual fairing of the normal acceleration due to presence of the superimposed oscillations. Hence, the normal acceleration was faired smooth, and linear lift curves were obtained in the region where flow separation is thought to have occurred.

Drag

Figure 8 presents data obtained from drag polars of which those shown in figure 7 are typical. Figure 8(a) shows the lift coefficient for minimum drag. The configuration had a value of $C_{L_{(C_{D_{min}})}}$ of approximately 0.09 for Mach numbers up to 0.95 but the value of this parameter decreased for the low supersonic Mach numbers. The minimum drag for the configuration is shown in figure 8(b) and has a value of 0.041 for Mach numbers below 0.9 increasing to 0.060 at a Mach number of 1.2. Comparison with the minimum drag for an identical configuration without the speed brake (ref. 1) shows that the speed brake accounted for approximately 55 percent of the minimum drag below a Mach number of 0.9 and 32 percent at a Mach number of 1.2. Figure 8(c) presents both the experimental and theoretical values of the drag-due-to-lift parameter $\frac{dC_D}{dC_L^2}$. The experimental values fall below the theoretical curve for no leading-edge suction $\left(\frac{1}{57.3C_{L_\alpha}}\right)$ and well above the curve for full leading-edge suction $\frac{1}{\pi A}$. For determination of the parameter $\frac{1}{57.3C_{L_\alpha}}$, average values of C_{L_α} were used.

Trim

The trim characteristics of the configuration are shown in figure 9 together with the lift coefficient for zero angle of attack. The trim data are compared with those for the model of reference 1 in order to show the effect of the speed brake. The present test model trimmed to negative angles of attack ranging from approximately -0.5° at Mach numbers of 0.7 and 1.3 to a maximum of -2.0° at a Mach number of 1.0. The trim lift coefficient was positive throughout the Mach number range of the test. The effect of the speed brake was to provide more positive trim characteristics amounting to roughly 1.0° to 1.5° increase in angle

of attack and a corresponding increase of slightly over 0.1 in trim lift coefficient. The lift coefficient for zero angle of attack was a maximum of about 0.2 near a Mach number of 0.96 and decreased for the lower and higher Mach numbers.

It can be seen in figure 9(b) that the shape of the curve of trim lift coefficient for the present test differs slightly from that for the test of reference 1. This is not thought to be an effect of the speed brake, but rather a result of the manner in which the referenced data were obtained. For the test of reference 1, $C_{L_{trim}}$ was obtained from the pitching-moment curve plotted against lift coefficient. This resulted in a limited number of values of $C_{L_{trim}}$ and in insufficient accuracy (due to hysteresis in the pitching-moment curves) to define accurately a trend as shown by the present test data. For the present test, $C_{L_{trim}}$ was obtained as the average values of envelopes of lift-coefficient time histories. This is the usual and more accurate method of obtaining this parameter.

Lift and Static Stability

Figure 10 presents the variation with Mach number of the lift-curve and pitching-moment-curve slopes. The C_{L_α} data are shown for two ranges of lift coefficients in the transonic speed range since it is evident from the basic lift curves in figure 7 that C_{L_α} decreases with increasing lift coefficient in this region. The maximum value of C_{L_α} is 0.10 near a Mach number of 0.94 for the lift-coefficient range from -0.2 to 0.2 and 0.086 near a Mach number of 0.9 for the lift-coefficient range from 0.2 to 0.4. The C_{L_α} data from the WADC test for an identical steel-wing model without the speed brake are shown for comparison, and are in good agreement with present test results for the lift-coefficient range from 0.2 to 0.4. The slightly higher value of C_{L_α} for the WADC test at Mach number 1.21 may be an effect of wing flexibility as a result of the lower dynamic pressure for the wind-tunnel test as shown in figure 5(b).

The curve of C_{m_α} in figure 10(b) was obtained from the periods and damping of the longitudinal oscillations and is therefore an average value for this parameter. The maximum static stability occurs near Mach number 0.97 where the value of C_{m_α} is -0.06 for the center-of-gravity location of 29.7 percent $\bar{c}$ ahead of the leading edge of $\bar{c}$.

The period of the longitudinal oscillations and the aerodynamic-center location with respect to the leading edge of the mean aerodynamic chord are shown in figure 11. The aerodynamic center was obtained from

the average C_{m_α} values and both sets of C_{I_α} data from figure 10, and also from the average slopes of the pitching-moment curves in figure 7. The WADC data compare favorably with the present test results which indicate that the aerodynamic-center travel was from approximately 27 percent of the mean aerodynamic chord for the subsonic Mach numbers to 42 percent near a Mach number of 1.2. It should be pointed out that the difference between the solid- and dashed-line curves for the aerodynamic-center locations is due only to the different values of C_{I_α} used in conjunction with the same average value of C_{m_α}; and, therefore, these curves do not necessarily show the true limits of the aerodynamic-center travel with lift coefficient. The purpose of presenting the data in this manner is to indicate that in the transonic speed range, the location of the aerodynamic center is highly dependent upon the lift coefficient.

Damping

Figure 12 presents the time for the longitudinal oscillations to damp to one-half amplitude, and the sum of the pitch damping derivatives, $C_{m_q} + C_{m_{\dot{\alpha}}}$. The time to damp to one-half amplitude decreases with increasing Mach number. The higher values of C_{I_α} from figure 10(a) were used for determination of the sum of the pitch-damping derivatives. Although unstable (positive) pitch damping is indicated in the transonic speed range, the pitch damping is a small portion of the total damping for this configuration and therefore has little effect on the time to damp to one-half amplitude. Use of the lower values of C_{I_α} for determination of the sum of the pitch-damping derivatives would indicate less severe pitch damping instability in the transonic speed range. The dashed portions of the damping curves were estimated from tests reported in references 1 and 2 since the amplitudes of the oscillations at the higher Mach numbers were insufficient to obtain accurate damping data. The purpose of estimating the total damping was to obtain values for the determination of C_{m_α}. (See equation given in fig. 10(b).)

Static Pressure

One purpose of the present test was to determine the position error for a static-pressure tube located at the tip of the vertical tail as shown in figure 1. Figure 13 shows that for Mach numbers up to about 1.25, the tube static pressure is higher than the free-stream pressure recorded by the radiosonde balloon. The position error for the tube is severe between Mach numbers of approximately 0.9 to 1.25 and the maximum error varied between 2.5 and 3 pounds per square inch between Mach numbers 1.1 and 1.2. Below Mach number 0.9, the error is moderate to small and

approaches the accuracy of the test data. From Mach number 1.25 to near the maximum Mach number, the error is also small and the tube static pressure is slightly lower than the free-stream pressure. Note that the same general pattern of pressure variation for the tube was repeated for the same Mach number range during accelerating and coasting flight. The severe dips in tube static pressure are a result of the pulse rockets firing ahead of the tube and have no significance except to show the effect on the static pressure of a disturbance of this type.

The effect of angle of attack on the tube static pressure is shown for several Mach numbers in figure 14. Angle of attack affects the static pressure most in the transonic region, and in this region the pressure is higher for decreasing than for increasing angles of attack. Little if any of this hysteresis should be due to pressure system lag, since this effect was calculated and the data were corrected accordingly. For the lower Mach numbers, static pressure is affected only slightly by changes in angle of attack.

SUMMARY OF RESULTS

A flight test was conducted between Mach numbers of 0.7 and 1.3 of a 1/10-scale steel-wing model of the Northrop MX-775A missile with leading-edge droop, leading-edge extensions, inboard trailing-edge flaps, a speed brake on the vertical tail, and a static-pressure tube at the tip of the vertical tail. The significant results of this investigation were as follows:

1. The minimum drag coefficient for the complete configuration was 0.041 at subsonic Mach numbers and increased to 0.060 at a Mach number of 1.2. The speed brake accounted for 55 percent of the subsonic value and 32 percent at a Mach number of 1.2. The lift coefficient for minimum drag was approximately 0.09 for Mach numbers up to 0.95 but decreased for the higher Mach numbers.

2. The speed brake improved the trim characteristics of the configuration by making the angle of attack 1° to 1.5° more positive and the lift coefficient approximately 0.1 more positive. This resulted in slightly positive trim lift coefficients, but negative trim angles of attack.

3. The maximum value of lift coefficient for zero angle of attack was approximately 0.2 near a Mach number of 0.96.

4. The maximum value of the lift-curve slope was 0.10 at Mach number 0.94. However, nonlinearities in the lift-curves indicated that in the transonic region, the lift-curve slope was considerably reduced for lift coefficients above 0.2.

[redacted]

5. Movement of the aerodynamic center was from approximately 27 percent of the mean aerodynamic chord at subsonic Mach numbers to approximately 42 percent at a Mach number of 1.2.

6. The sum of the pitch-damping derivatives was unstable (positive) in the transonic region, but this had little effect on the total damping which was stable throughout the Mach number range of the test.

7. The location of the static-pressure tube resulted in severe errors in static pressure between Mach numbers of approximately 0.9 and 1.25. Below Mach number 0.9, the error was moderate to small.

Langley Aeronautical Laboratory,
National Advisory Committee for Aeronautics,
Langley Field, Va., January 26, 1955.

Richard G. Arbic
Aeronautical Research Scientist

Approved:

Joseph A. Shortal
Chief of Pilotless Aircraft Research Division

mgk

[redacted]

REFERENCES

1. Arbic, Richard G.: Free-Flight Investigation of the Low-Lift Transonic Aerodynamic Characteristics of a 1/10-Scale Model of the Northrop MX-775A With an Aluminum-Alloy Wing Having Leading-Edge Extensions and Inboard Trailing-Edge Flaps. NACA RM SL54E10, U. S. Air Force, 1954.

2. Arbic, Richard G., and Gillespie, Warren, Jr.: Free-Flight Longitudinal-Stability Investigation Including Some Effects of Wing Elasticity From Mach Numbers of 0.85 to 1.34 of a Tailless Missile Configuration Having a 45° Sweptback Wing of Aspect Ratio 5.5. NACA RM L53F18, 1953.

3. Gillespie, Warren, Jr., and Arbic, Richard G.: Large-Scale Flight Measurements of Zero-Lift Drag at Mach Numbers From 0.87 to 1.39 of 1/10-Scale Models of the Northrop MX-775A Missile. NACA RM SL51K07, U. S. Air Force, 1951.

4. Wolford, Russell D.: Report of a Series of Wind-Tunnel Tests on a 1/13-Scale Model of the XSSM-A-3a Snark in the Wright Field 10-Foot Wind-Tunnel. Tech. Note WCLS 53-29 (RDO No. 448-47), Wright Air Dev. Center, U. S. Air Force, March 24, 1953.

5. Phelps, E. Ray, and Lazzeroni, Frank A.: Wind-Tunnel Investigation of the Aerodynamic Characteristics of a 1/15-Scale Model of the Northrop MX-775A Missile. NACA RM A51E28, 1951.

6. Gillis, Clarence L., Peck, Robert F., and Vitale, A. James: Preliminary Results From a Free-Flight Investigation at Transonic and Supersonic Speeds of the Longitudinal Stability and Control Characteristics of an Airplane Configuration With a Thin Straight Wing of Aspect Ratio 3. NACA RM L9K25a, 1950.

[redacted]

TABLE I

PHYSICAL CHARACTERISTICS OF THE MODEL

Modified wing:	
Area, sq ft	3.65
Basic wing:	
Area, sq ft	3.27
Span, ft	4.23
Aspect ratio	5.5
Mean aerodynamic chord, ft	0.82
Sweepback of 0.406-chord line, deg	45
Dihedral, deg	0
Taper ratio, Tip chord/Root chord	0.4
Vertical tail:	
Area (extended to center line), sq ft	0.45
Span (from fuselage center line), ft	1
Sweepback of 0.4-chord line, deg	33
Taper ratio	0.286
Fuselage:	
Length, ft	6.74
Maximum diameter, ft	0.483
Fuselage fineness ratio, Length/Diameter	13.94
Nose fineness ratio	4.14
Boattail fineness ratio	2.76
Weight and balance:	
Weight, lb	121.5
Wing loading, (modified wing), lb/sq ft	33.3
Center of gravity position, percent $\bar{c}$ forward of leading edge of $\bar{c}$	29.7
Moment of inertia in pitch, I_y, slug-ft^2	8.85

TABLE II

BODY AND AIRFOIL ORDINATES

Body ordinates		Ordinates for basic wing, percent chord			Vertical-tail ordinates, percent chord		Ordinates for modified wing, percent chord (a)		
Station, in. from nose	Radius, in.	Station	Upper	Lower	Station	Upper and Lower	Station	Upper	Lower
0	0	0	-0.850	-0.850	0	0	0.	-1.70	-1.70
1.4	.380	1.25	.200	-1.573	1.25	.960	.10	-1.39	-2.00
2.0	.548	2.50	.610	-1.855	2.50	1.335	.76	-.73	-2.37
4.0	1.066	5.00	1.120	-2.190	5.00	1.770	3.12	.03	-2.68
6.0	1.502	7.50	1.480	-2.410	7.50	2.060	5.49	.68	-2.76
8.0	1.857	10.00	1.773	-2.567	10.00	2.265	7.85	1.18	-2.76
10.0	2.151	15.00	2.227	-2.782	15.00	2.567	10.23	1.59	-2.72
12.0	2.390	20.00	2.532	-2.922	20.00	2.770	12.78	1.94	-2.68
14.0	2.575	25.00	2.747	-2.998	25.00	2.907	14.96	2.10	-2.76
17.0	2.770	30.00	2.900	-3.033	30.00	3.010	17.33	2.24	-2.83
20.0	2.878	35.00	2.980	-3.040	40.00	3.120	19.68	2.37	-2.88
22.0	2.900	40.00	3.010	-3.020	50.00	3.057	22.05	2.49	-2.91
Straight line		50.00	2.855	-2.860	60.00	2.810	24.42	2.60	-2.94
65.0	2.900	60.00	2.380	-2.380	70.00	2.395	26.80	2.68	-2.96
68.0	2.875	70.00	1.812	-1.812	75.00	2.090	29.15	2.75	-2.98
70.0	2.810	80.00	1.233	-1.233	Straight line		33.90	2.84	-2.98
72.0	2.700	90.00	.640	-.640	100.00	.100	38.56	2.89	-2.96
74.0	2.545	100.00	.015	-.015			43.40	2.87	-2.90
76.0	2.340						48.05	2.78	-2.81
78.0	2.070						52.90	2.66	-2.64
80.0	1.710						57.50	2.39	-2.40
80.9	1.500						62.20	2.13	-2.14
							67.50	1.85	-1.89
							71.70	1.27	-2.23
							76.50	.59	-2.62
							81.20	-.09	-2.99
							83.10	-.36	-3.12
							85.90	-.77	-3.10
							90.70	-1.44	-3.06
							95.20	-2.11	-3.00
							100.00	-2.79	-2.91

[a]Ordinates as measured on right wing panel at 0.355b/2. Percentages based on local chord length of 10.58 inches.

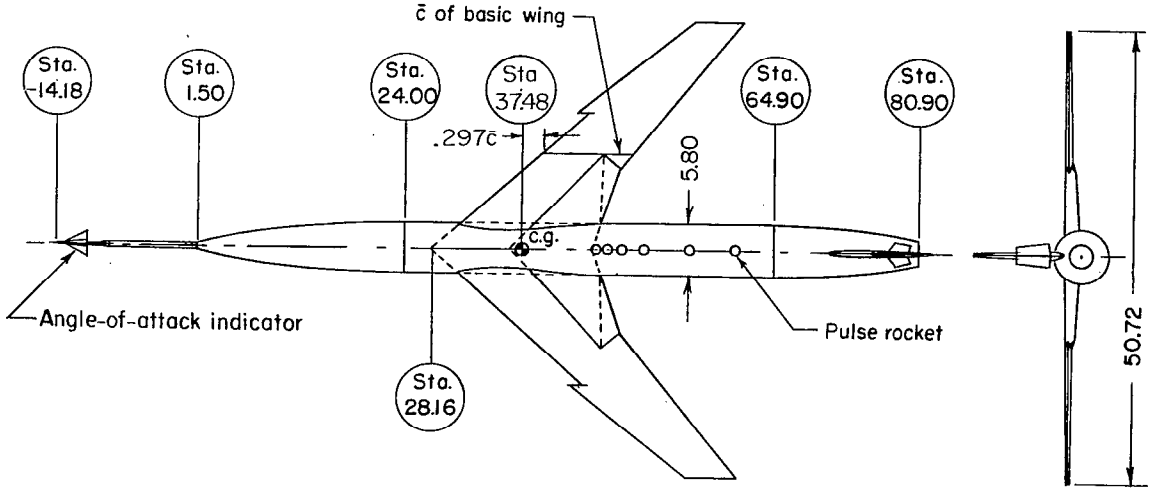

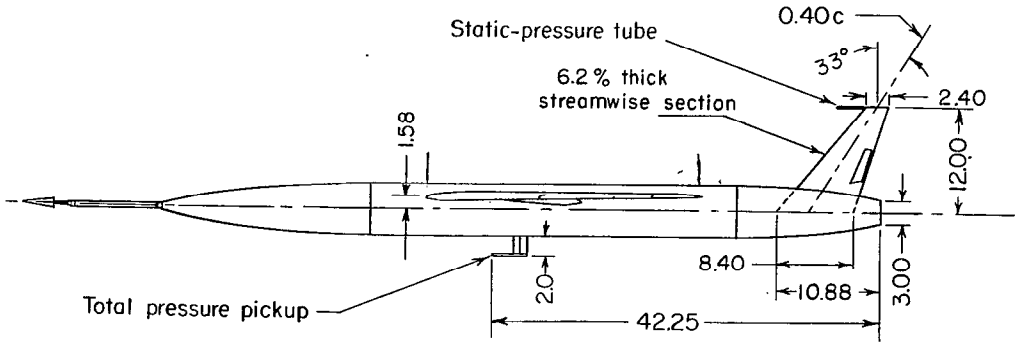

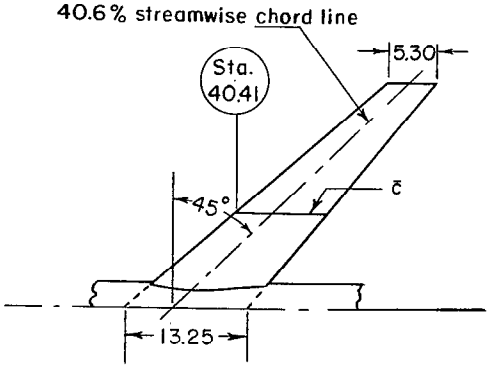

Detail of basic wing

Note:

Airfoil section is modified NACA 65-009 normal to 0.406 streamwise chord line.

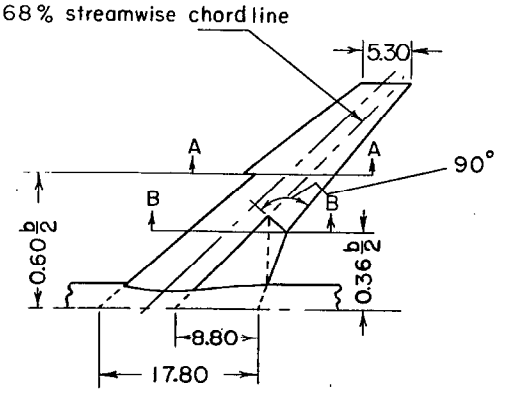

Detail of modified wing

Note: 1. L.E. extension is 15% of basic-wing streamwise chord at 60% semispan.
2. Forward 15% of L.E. deflected 7° down streamwise.
3. T.E. flap deflected 5° down streamwise.

Figure 1.- General arrangement of the model. All dimensions are in inches.

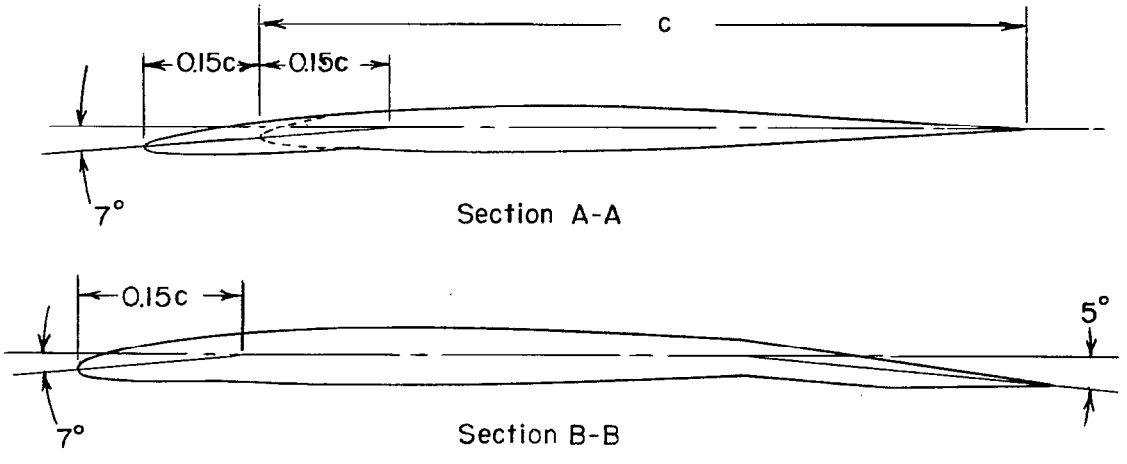

Sections of the modified airfoil

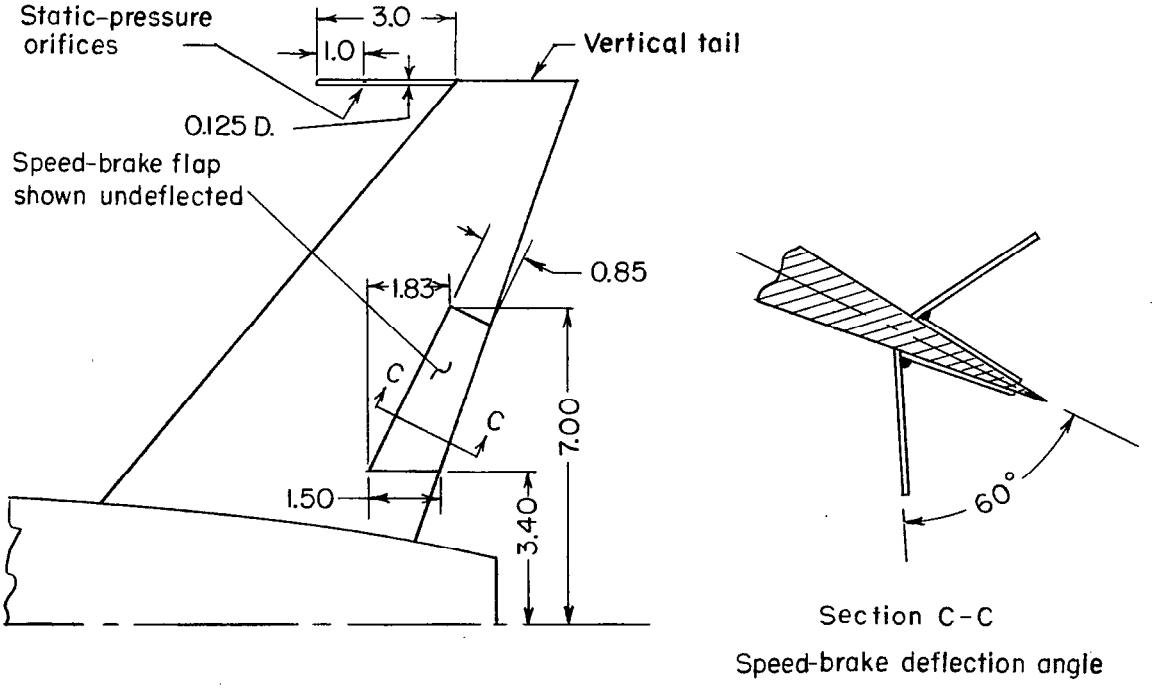

Speed-brake and static-pressure-tube details

Figure 1.- Concluded.

L-84425

Figure 2.- Photograph of the model.

L-84687.2

Figure 3.- Model-booster combination prior to launching.

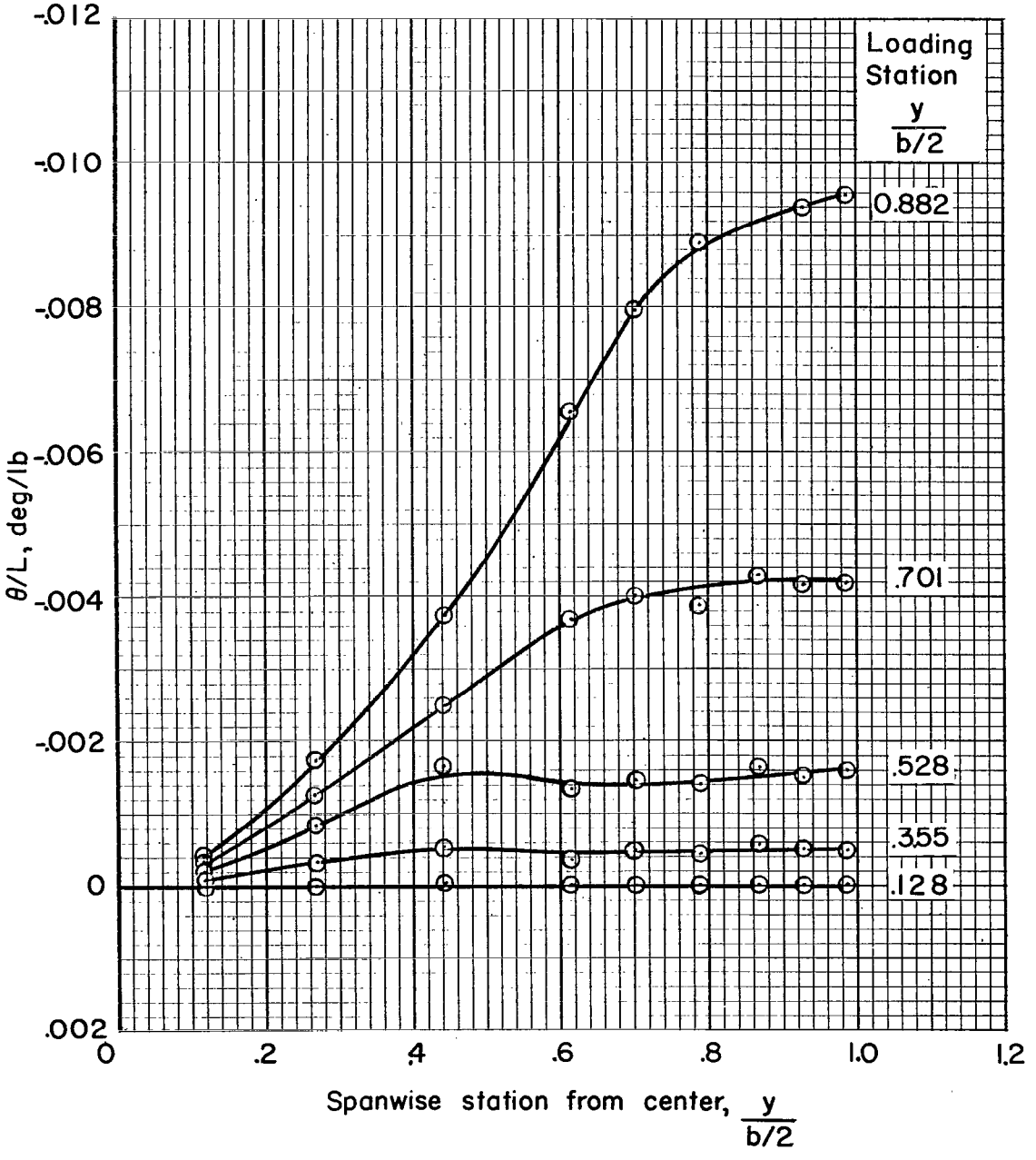

Figure 4.- Streamwise angle of twist per unit load for the steel wing due to loads applied along the 40-percent-streamwise-chord line and at the spanwise stations indicated.

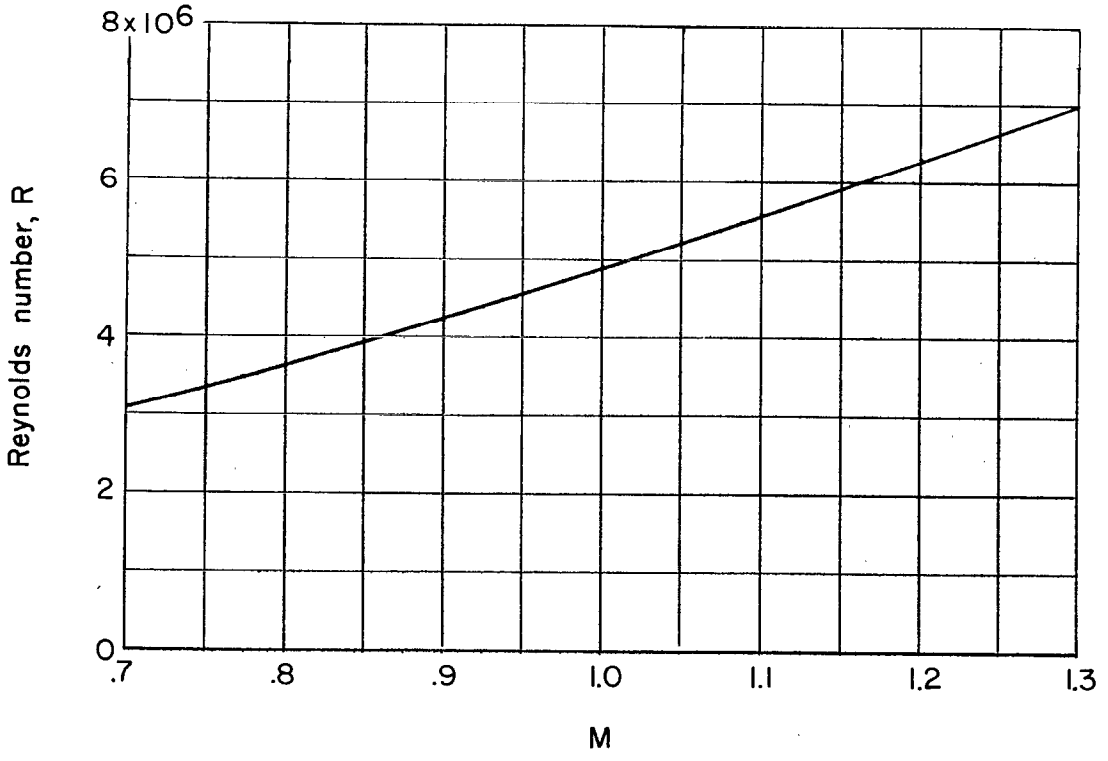

(a) Reynolds number.

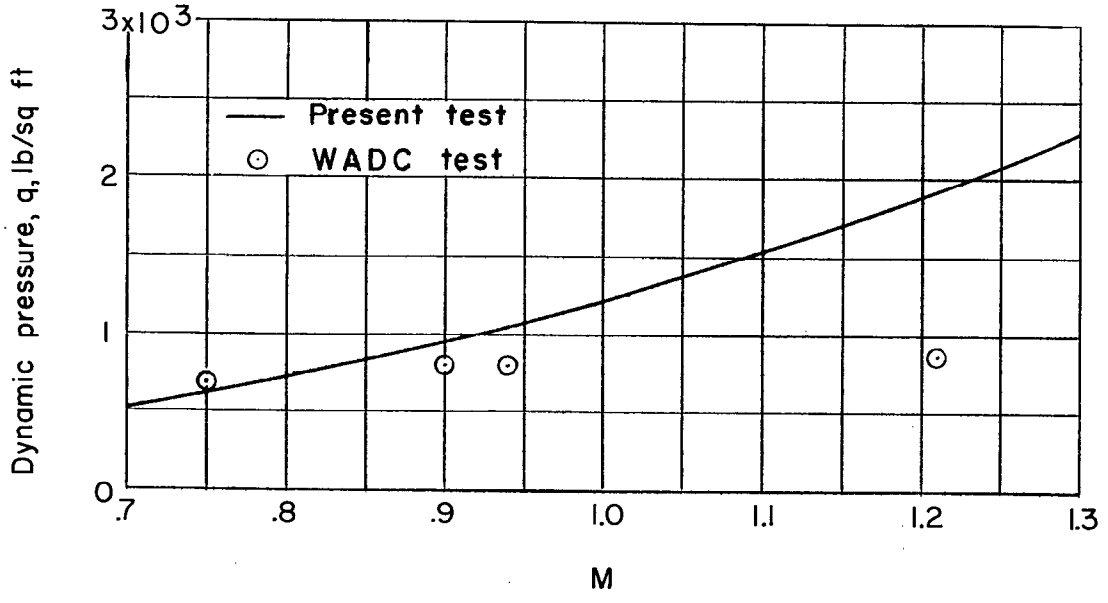

(b) Dynamic pressure.

Figure 5.- Test conditions of Reynolds number and dynamic pressure.

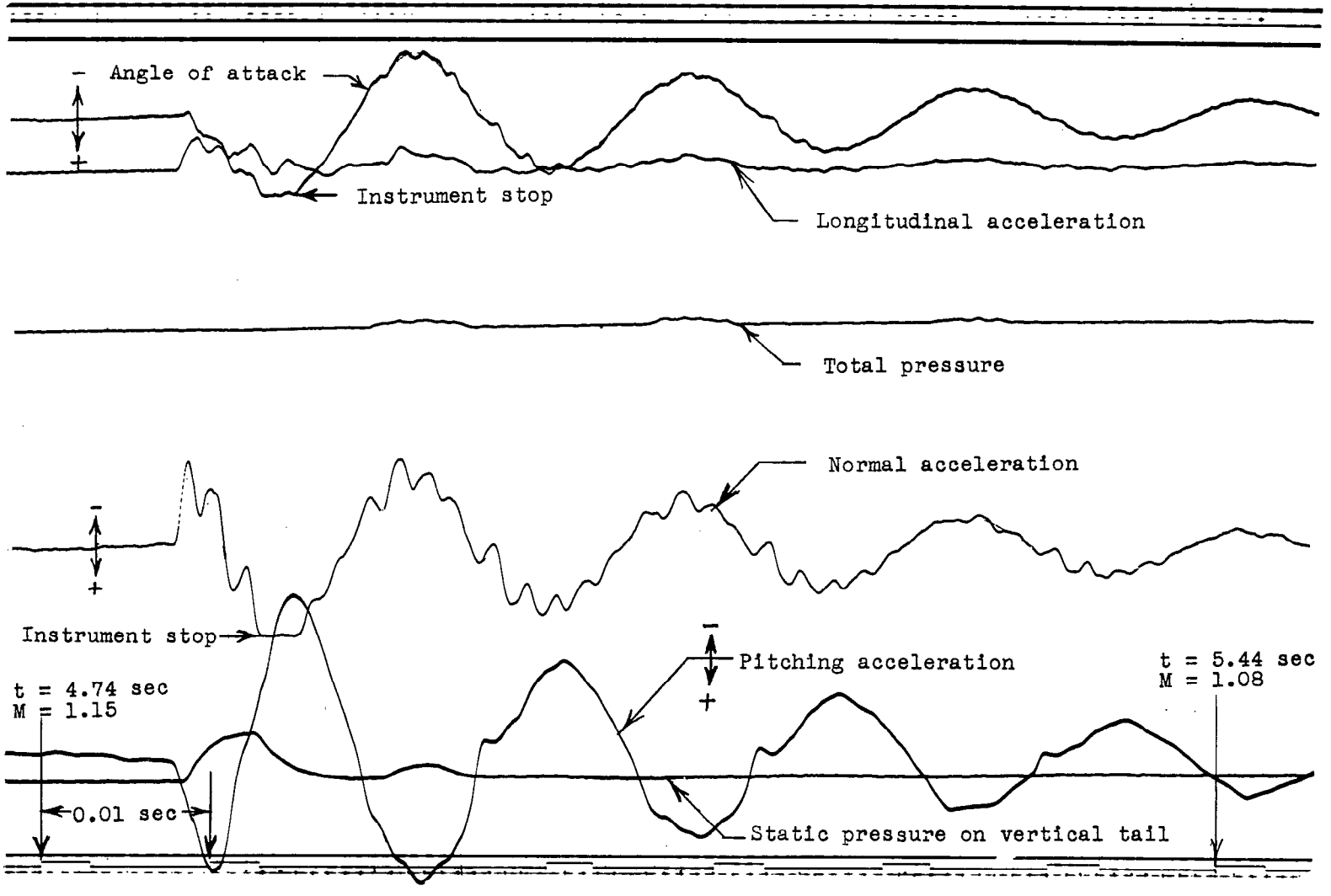

Figure 6.- Portion of the telemeter record.

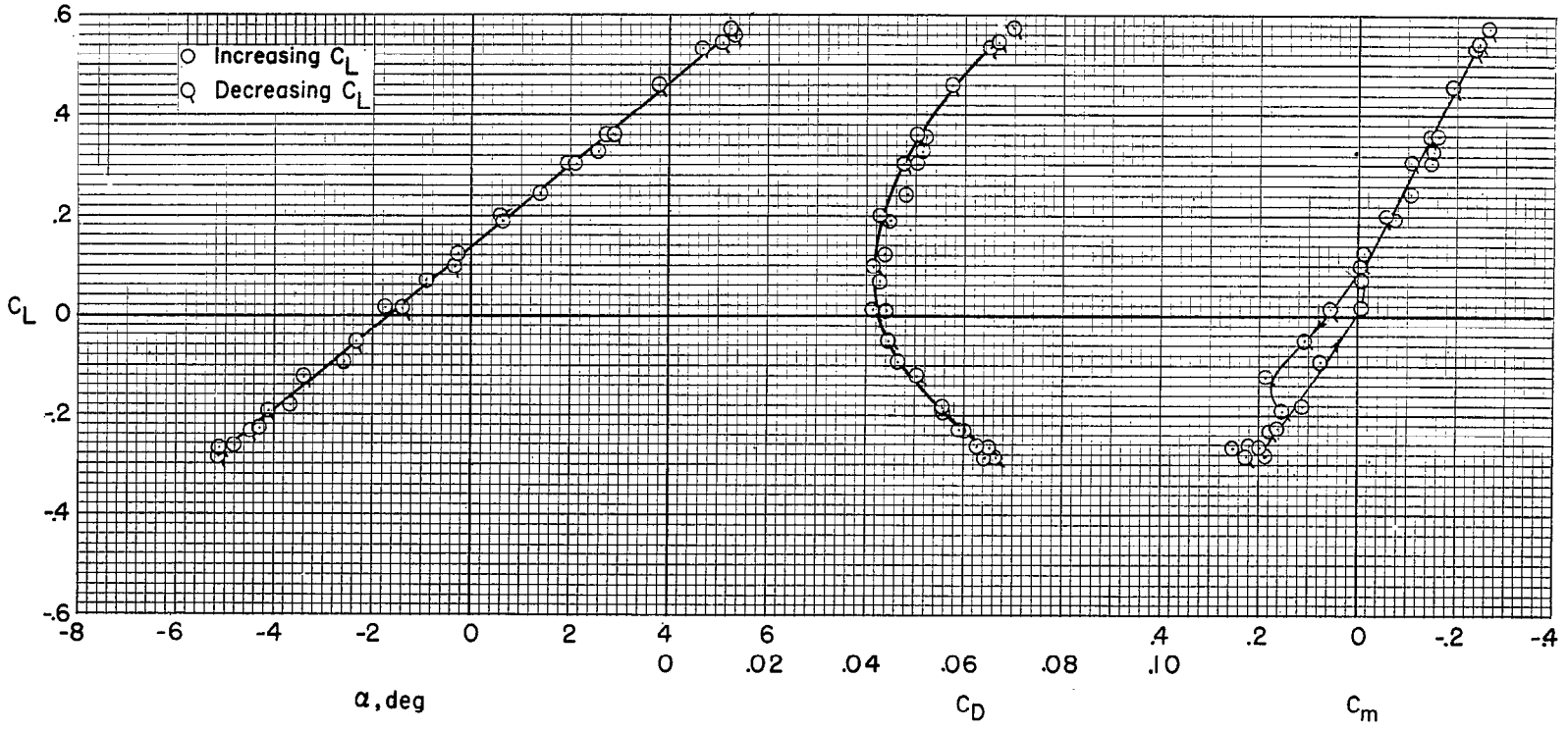

(a) M = 0.758.

Figure 7.- Typical basic lift, drag, and pitching-moment data.

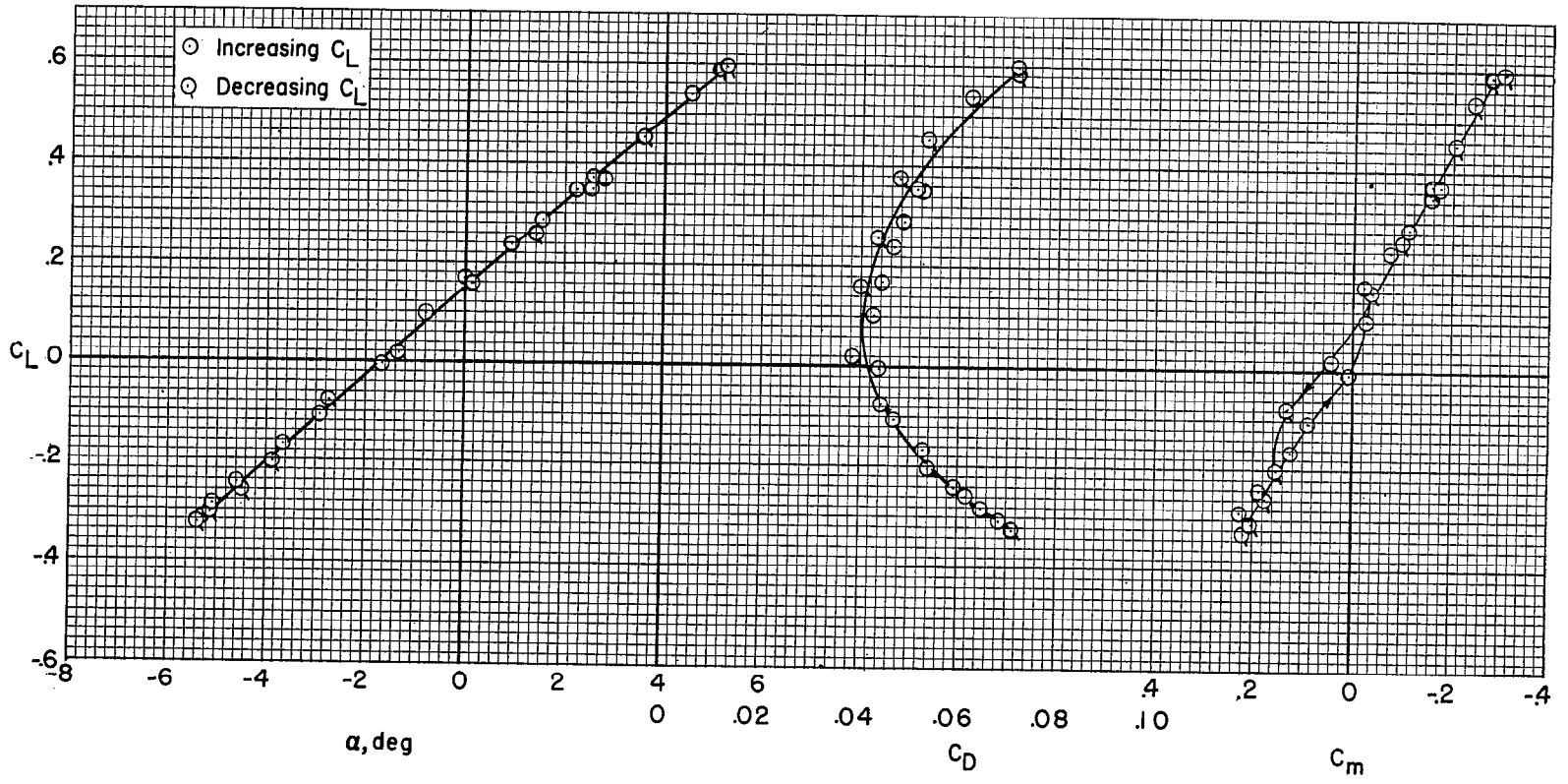

(b) M = 0.818.

Figure 7.- Continued.

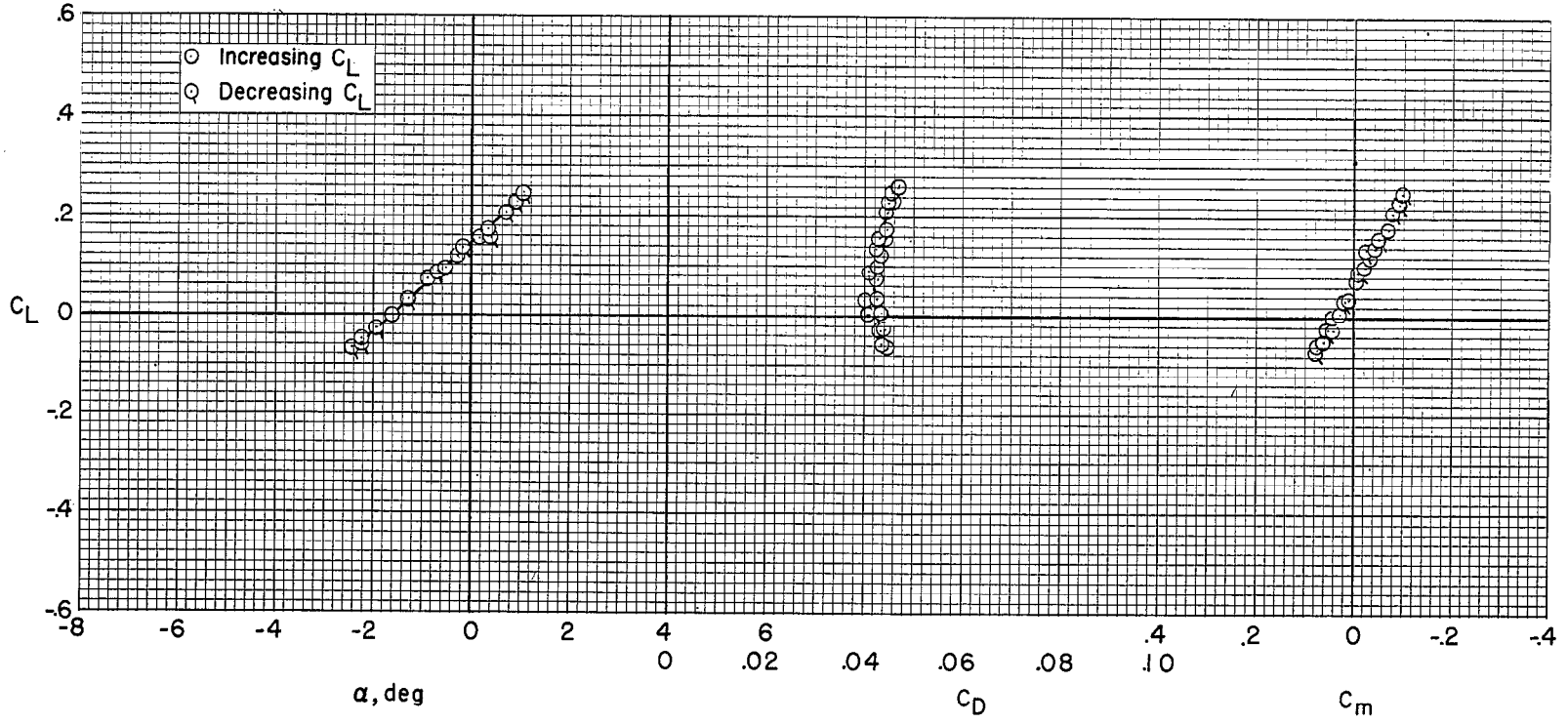

(c) M = 0.856.

Figure 7.- Continued.

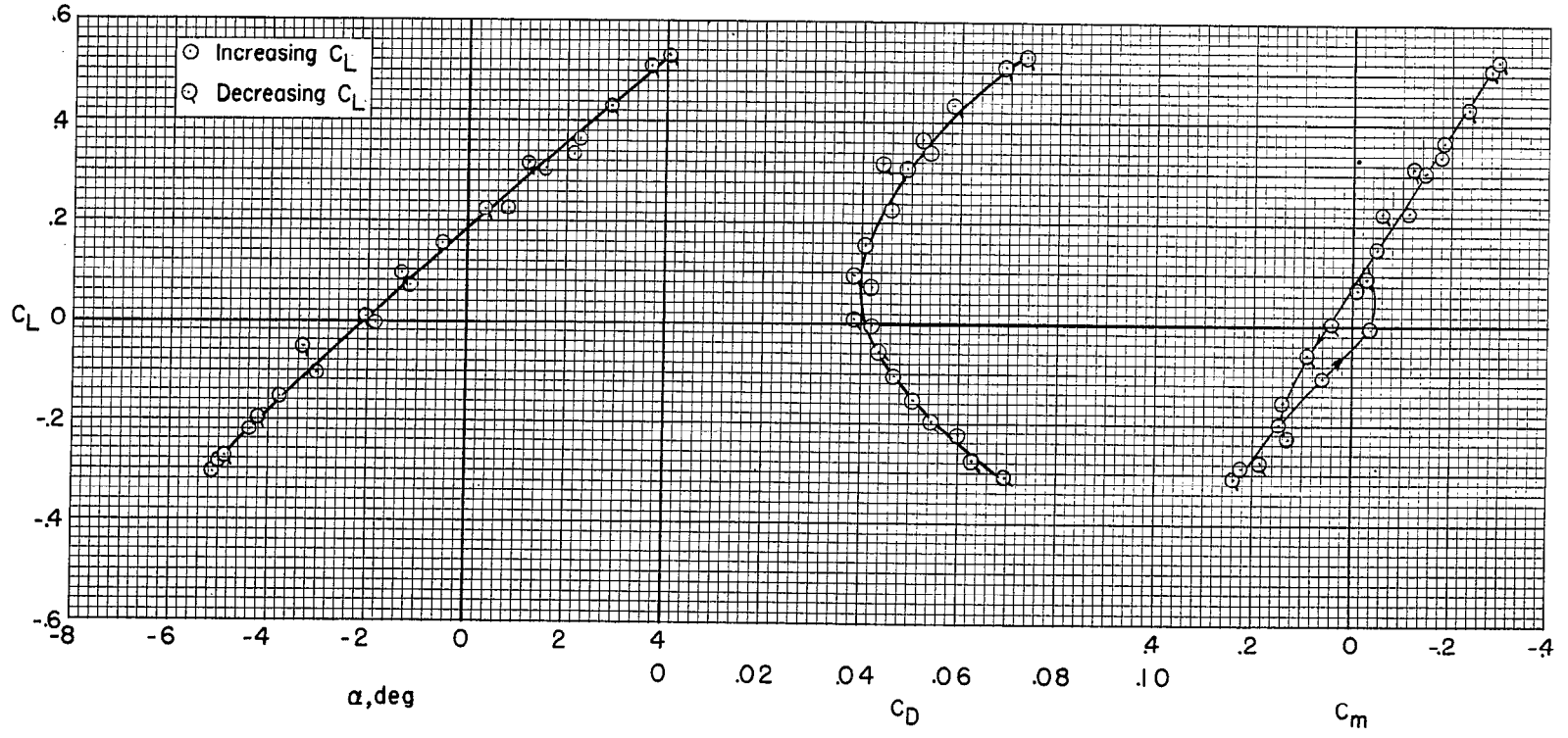

(d) M = 0.884.

Figure 7.- Continued.

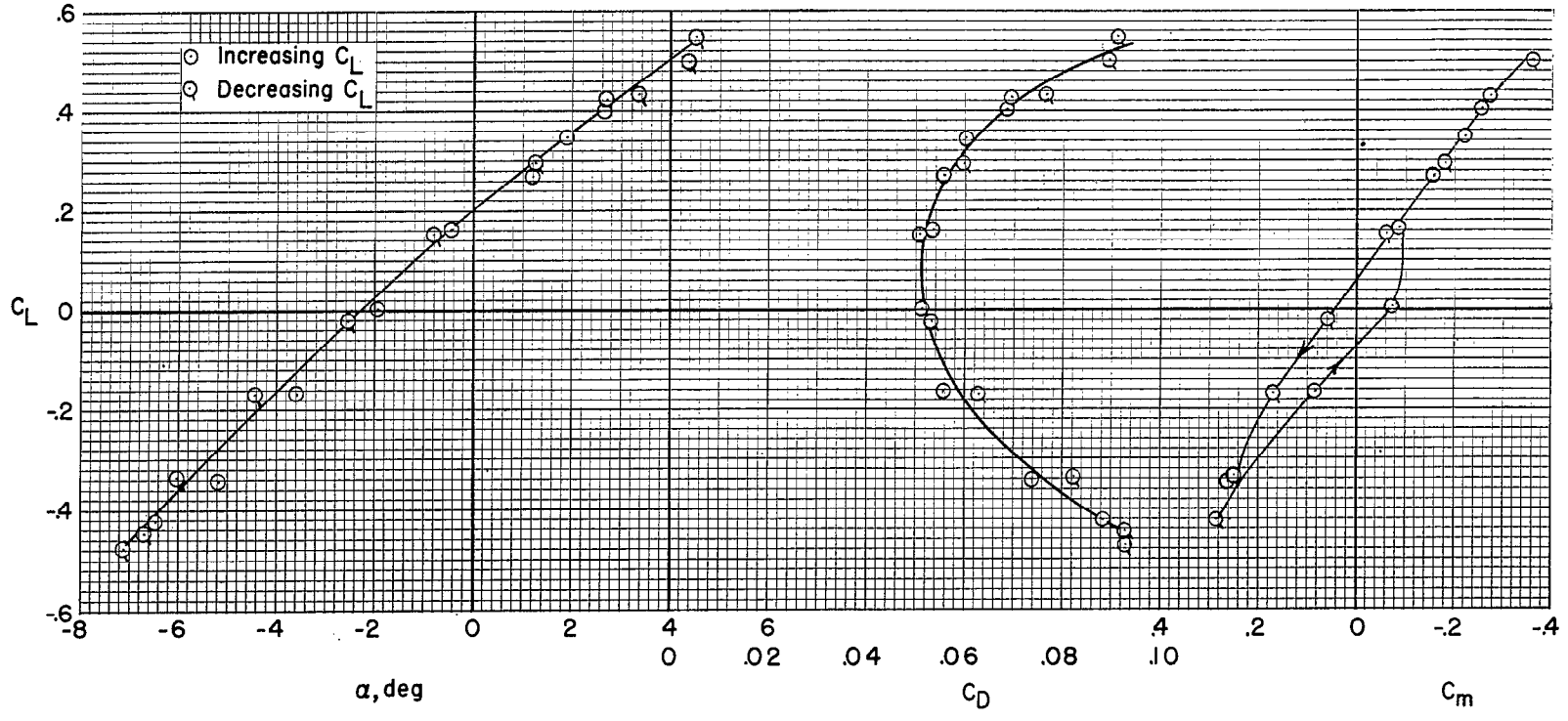

(e) M = 0.961.

Figure 7.- Continued.

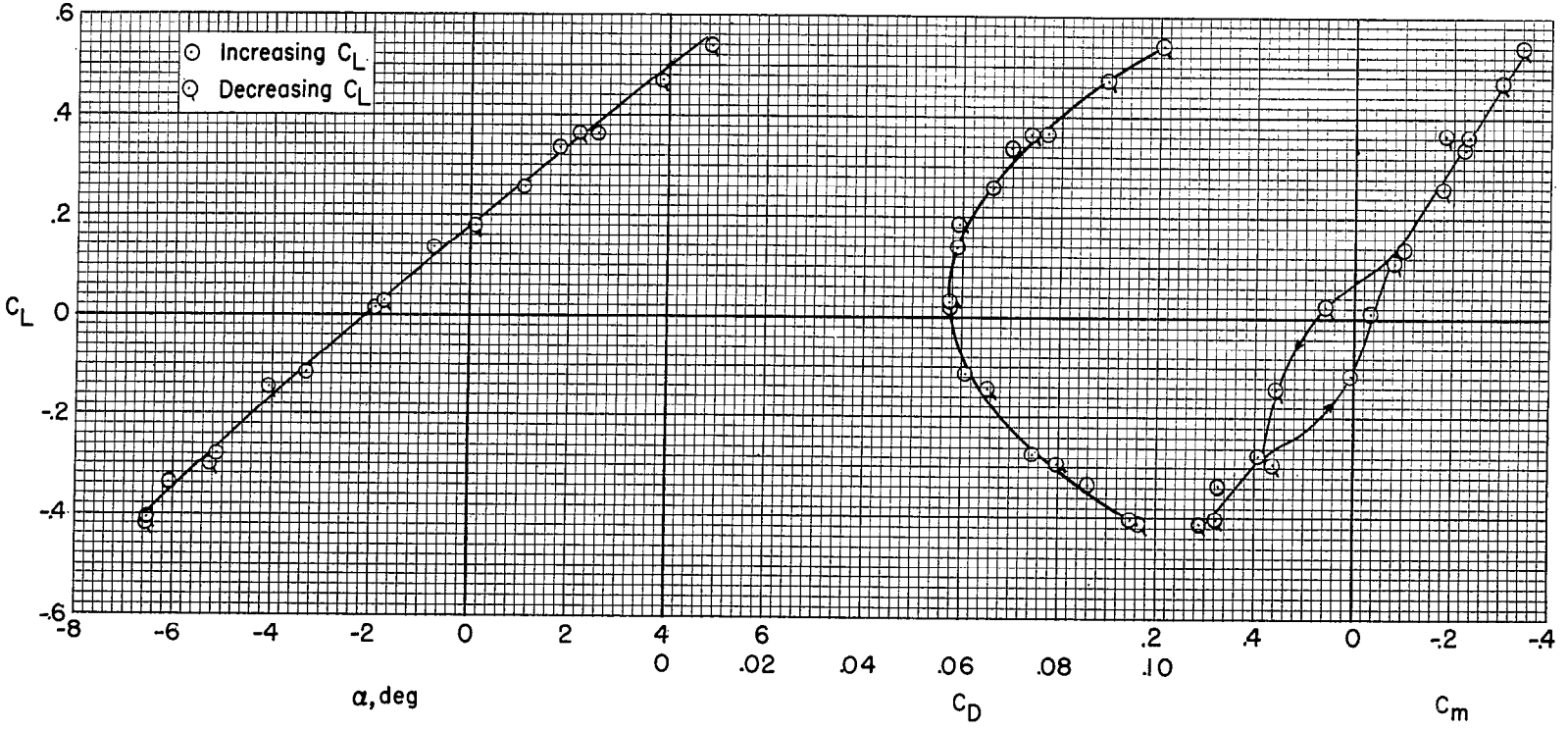

(f) M = 1.040.

Figure 7.- Continued.

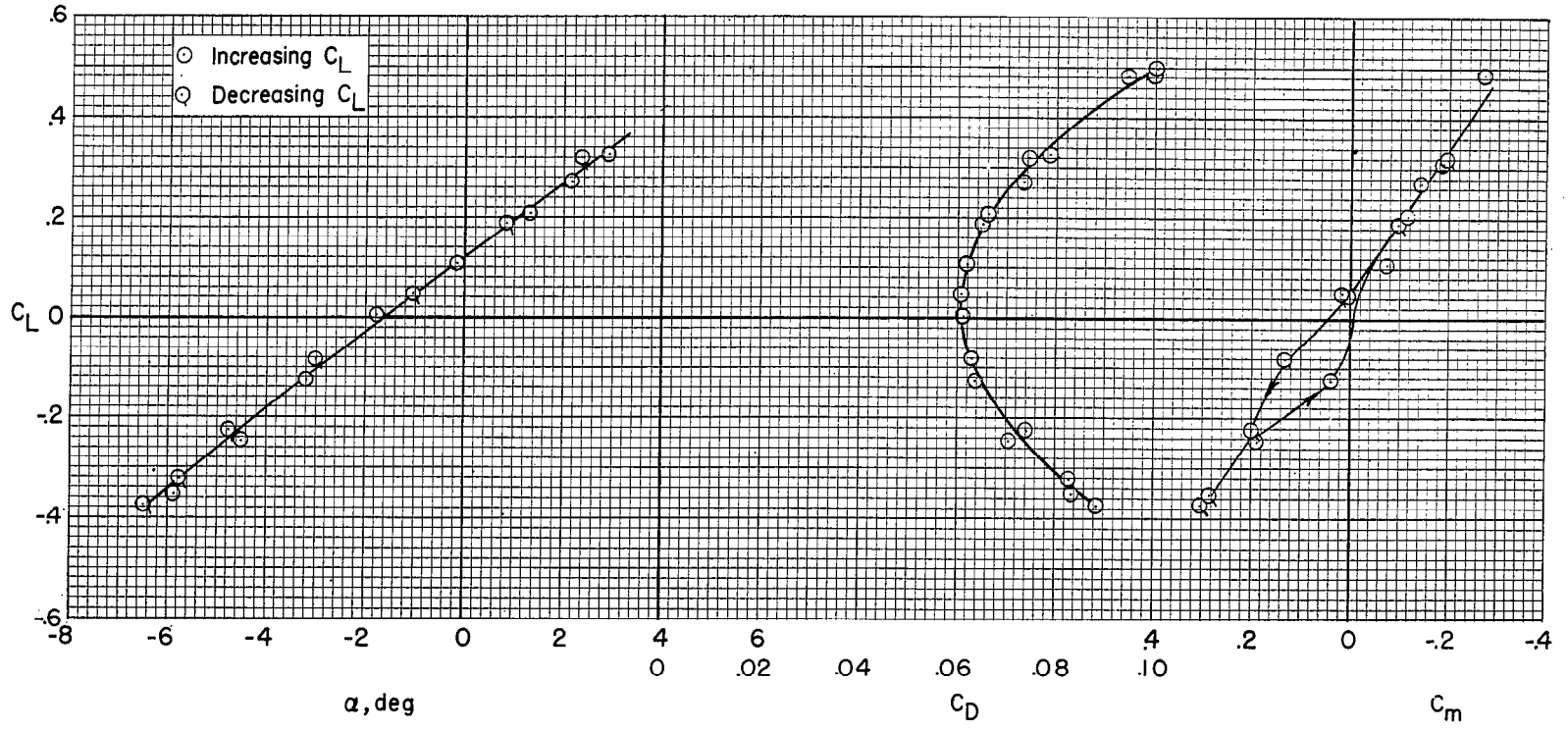

(g) M = 1.125.

Figure 7.- Concluded.

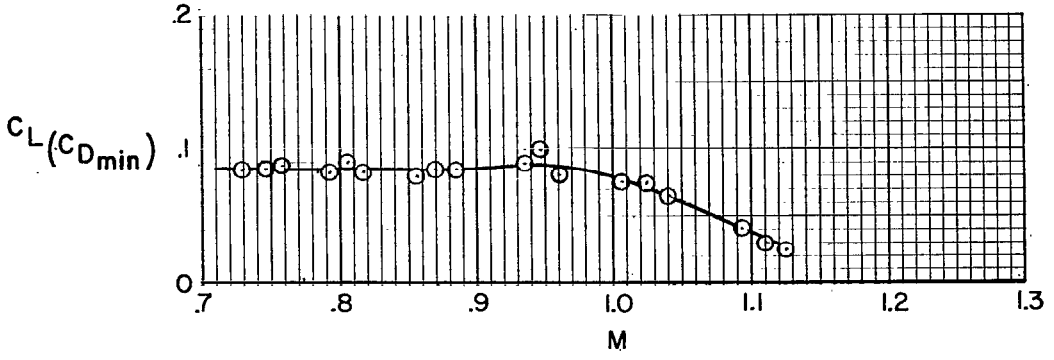

(a) C_L for $C_{D_{min}}$.

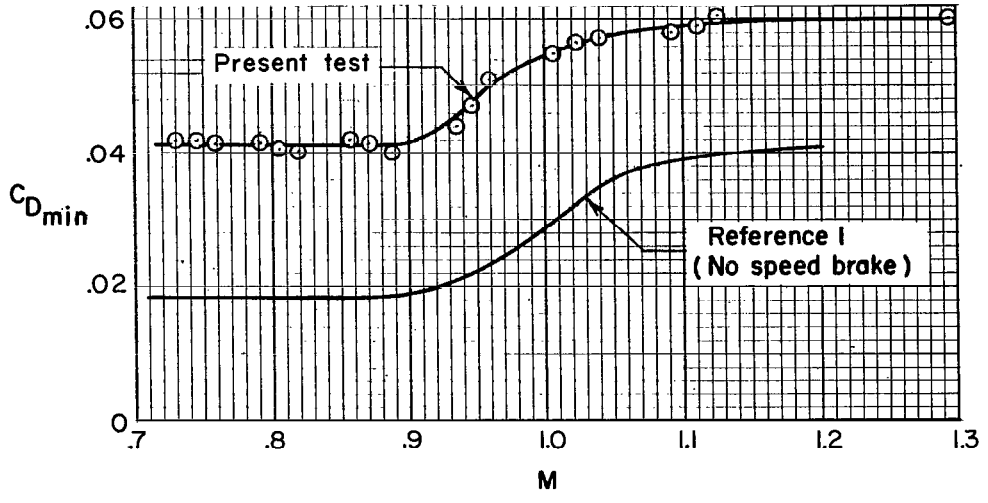

(b) Minimum drag coefficient.

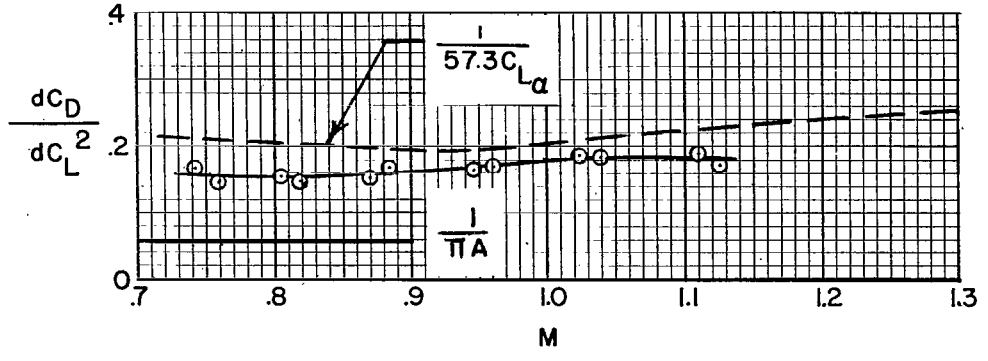

(c) Drag due to lift.

Figure 8.- Drag data.

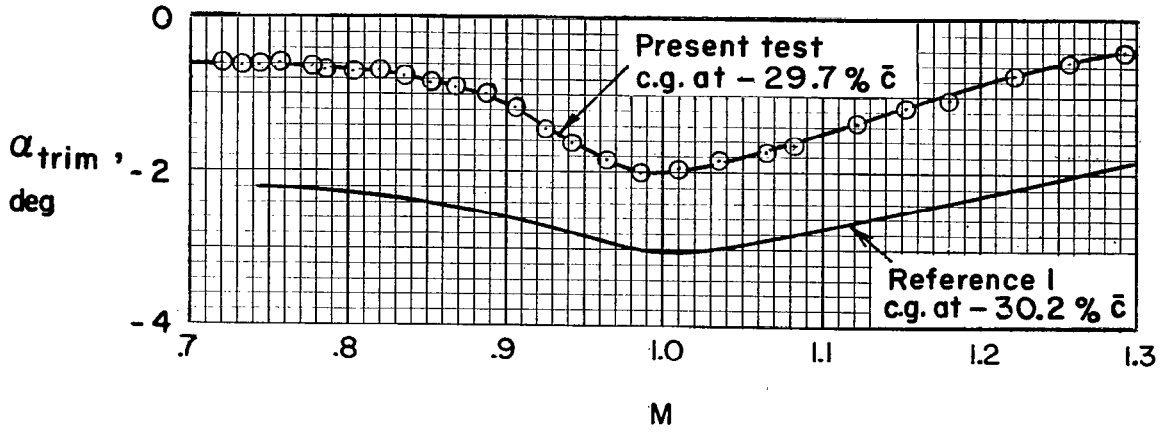

(a) Trim angle of attack.

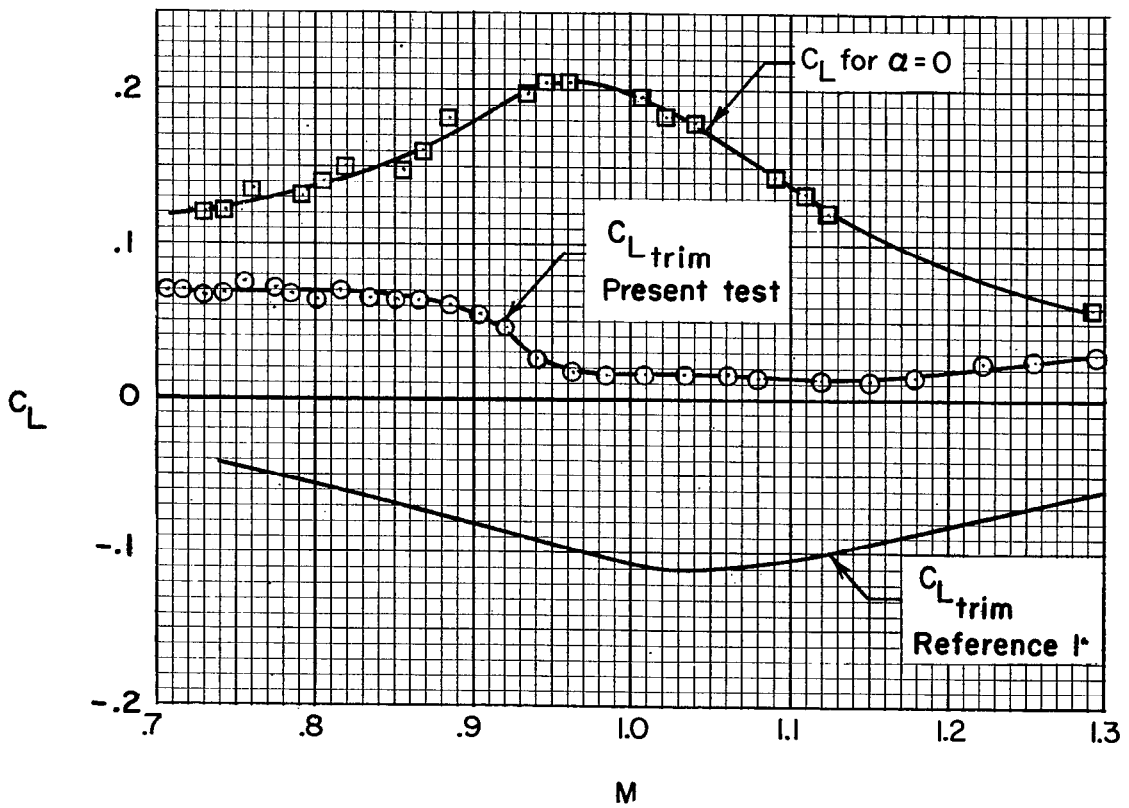

(b) Trim C_L and C_L for $\alpha = 0$.

Figure 9.- Data at trim and for $\alpha = 0$. Model of reference 1 had no speed brake.

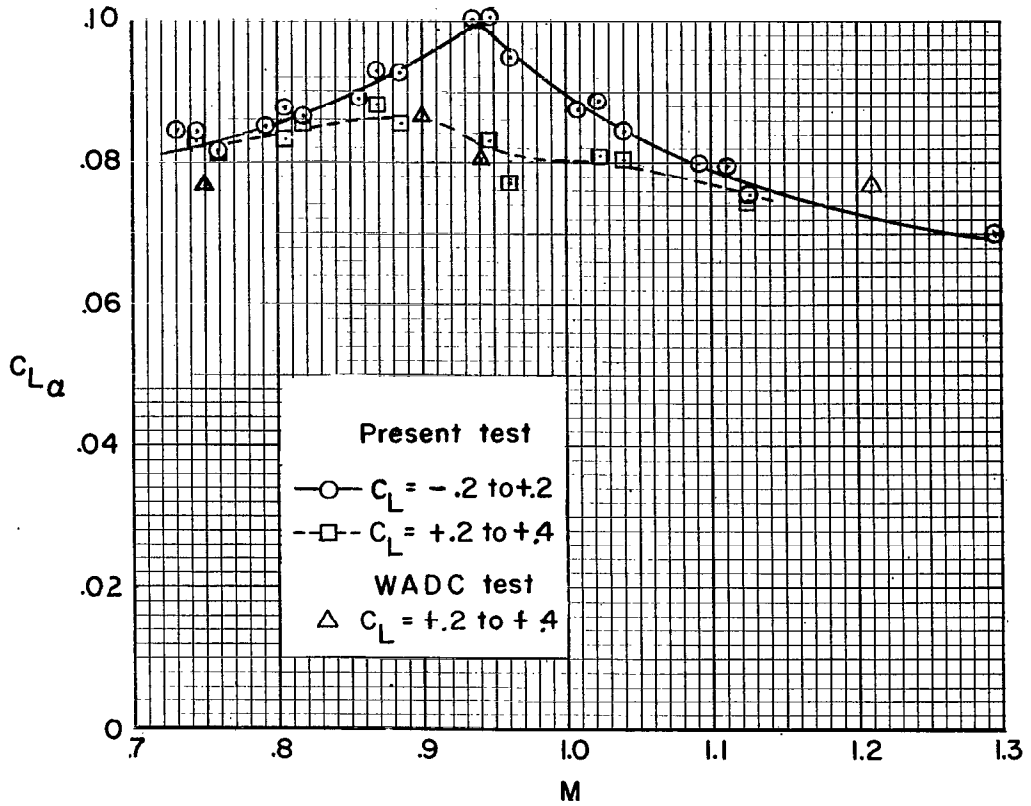

(a) Lift-curve slope.

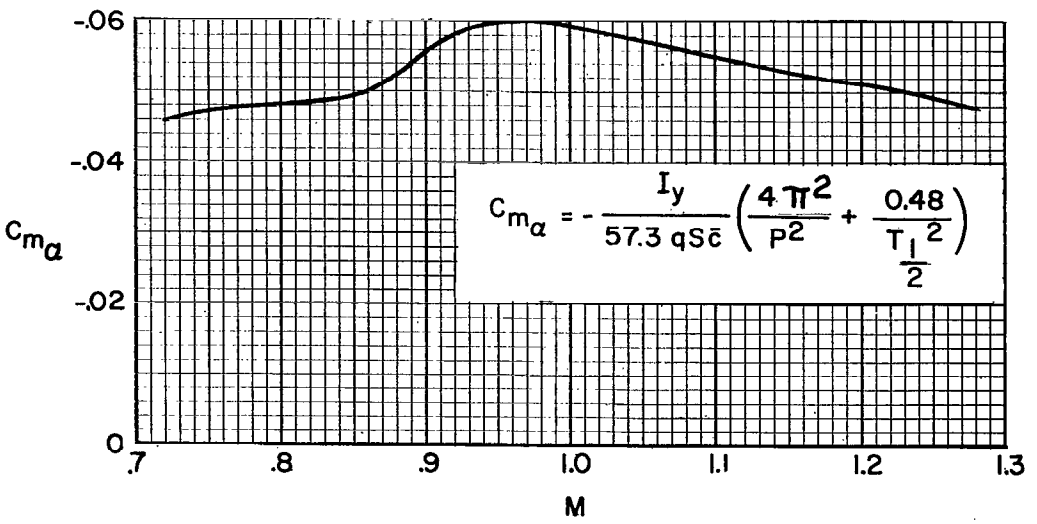

(b) Pitching-moment-curve slope.

Figure 10.- Lift-curve and pitching-moment-curve slopes.

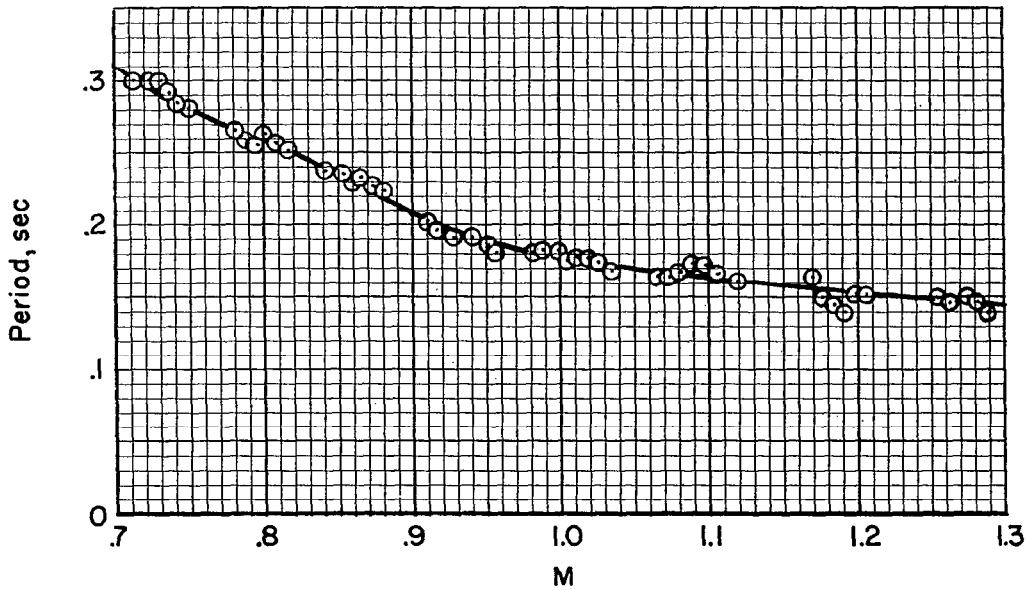

(a) Period of the longitudinal oscillation.

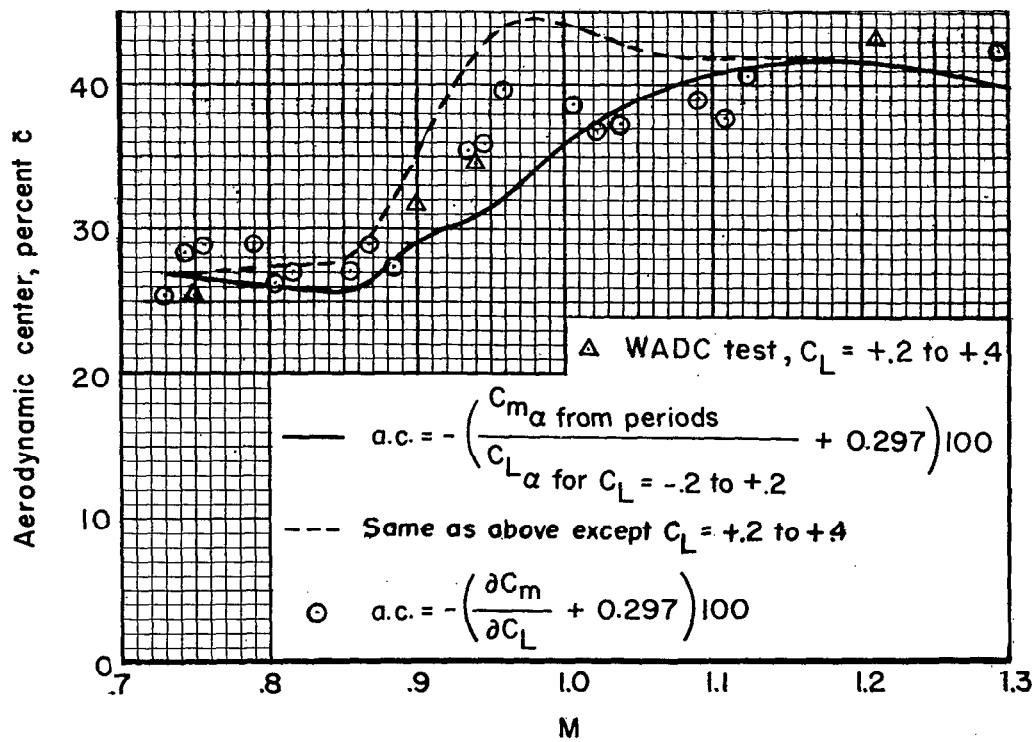

(b) Aerodynamic center.

Figure 11.- Period and aerodynamic center.

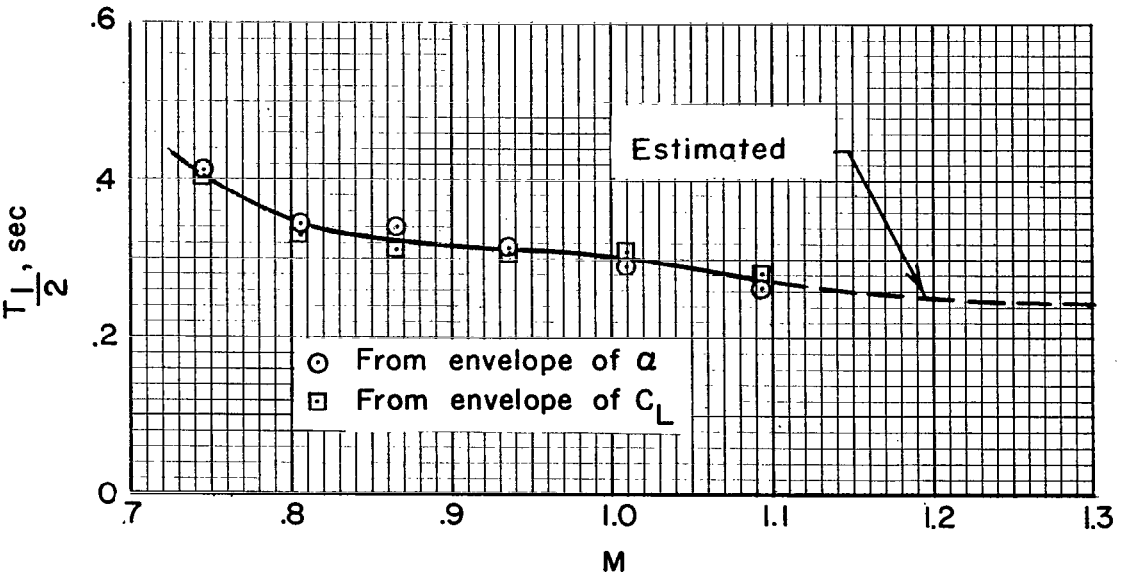

(a) Time to damp to one-half amplitude.

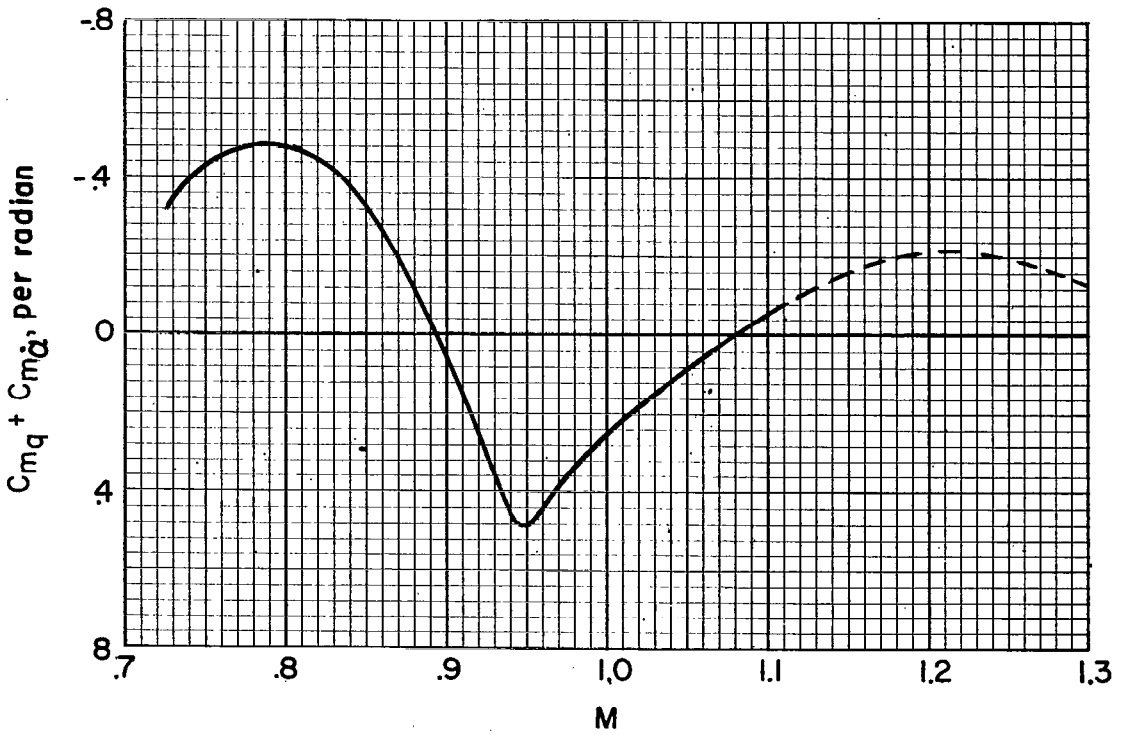

(b) Pitch-damping coefficients.

Figure 12.- Variation of total-damping and pitch-damping with Mach number.

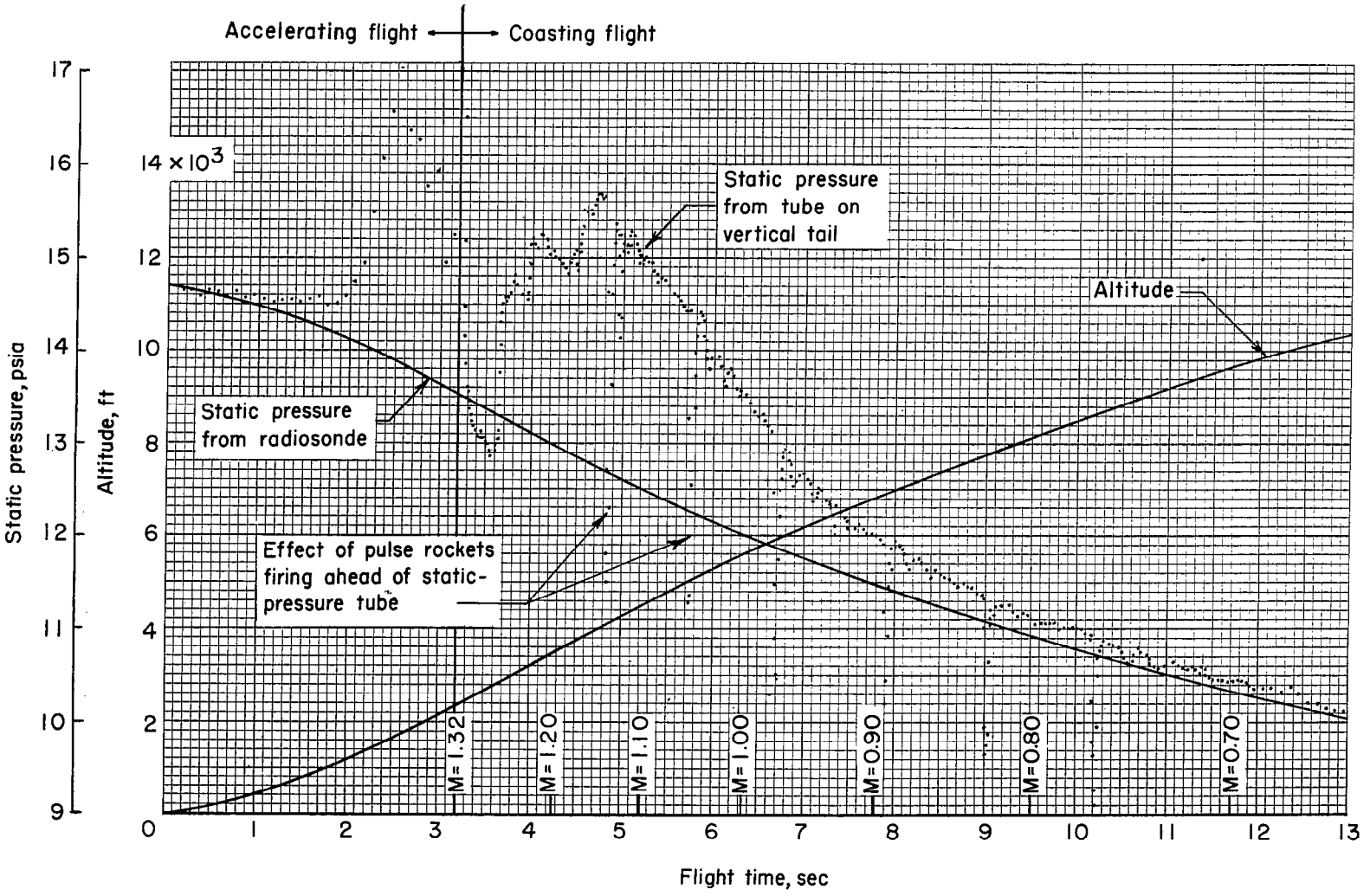

Figure 13.- Time histories of altitude and of static pressure from the radiosonde and the static-pressure tube.

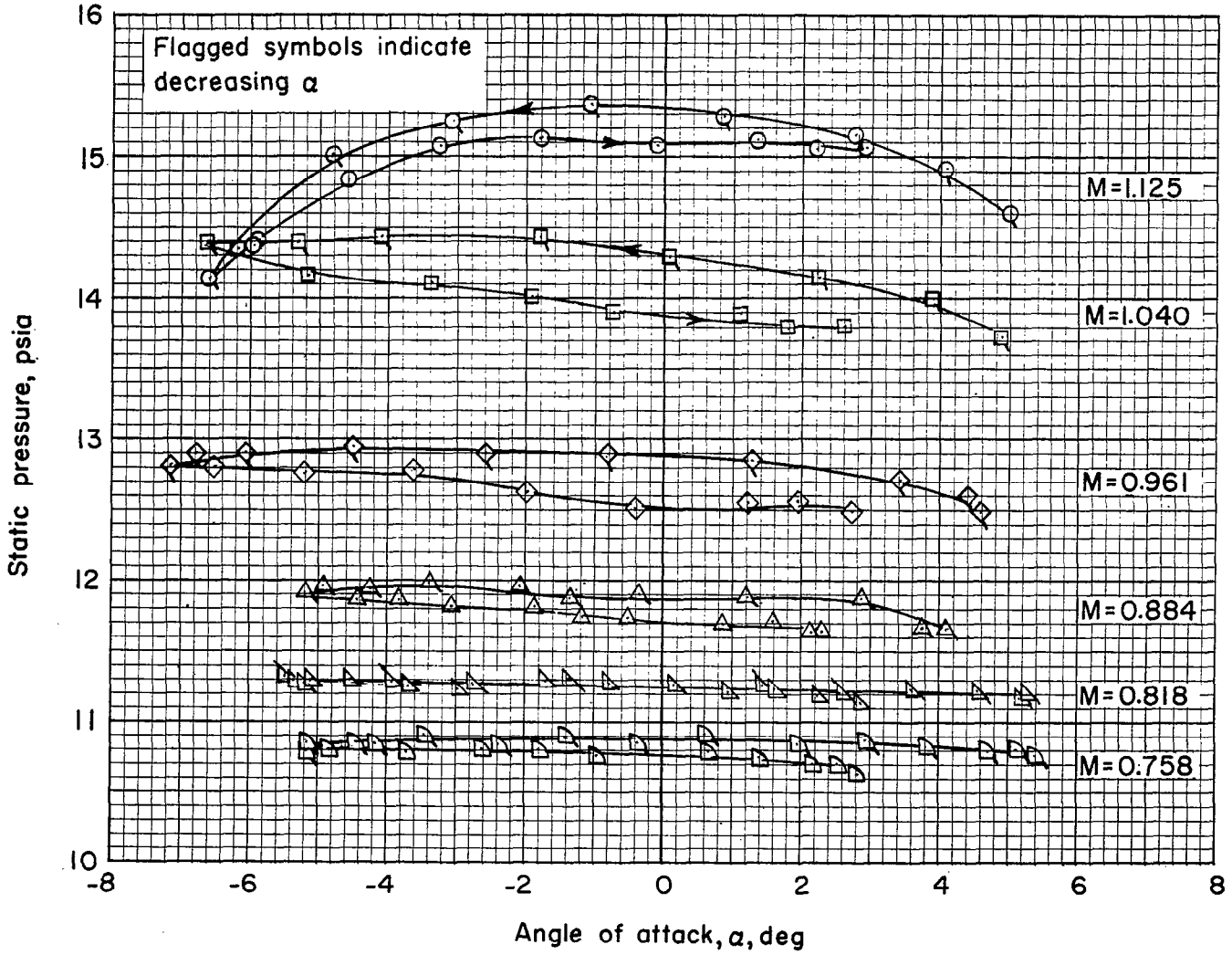

Figure 14.- Variation of tube static pressure with angle of attack for various Mach numbers.